THE FLORIDA STATE UNIVERSITY

COLLEGE OF ARTS AND SCIENCES

DEVELOPMENT OF SCATTEROMETER-DERIVED RESEARCH-QUALITY

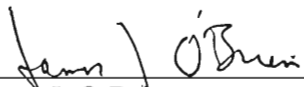SURFACE PRESSURES FOR THE SOUTHERN OCEAN

By

KYLE A. HILBURN

A Thesis submitted to the
Department of METEOROLOGY
in partial fulfillment of the
requirements for the degree of
Master of Science
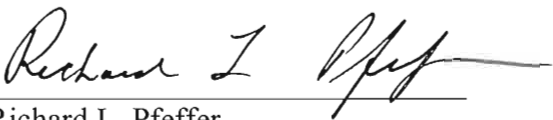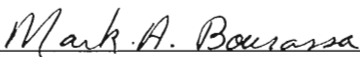
Degree Awarded:
Summer Semester, 2002

The members of the Committee approve the thesis of

Kyle A. Hilburn defended on June 4, 2002.

_____

James J. O Brien
Professor Directing Thesis

_____

Guosheng Liu
Committee Member

_____

Richard L. Pfeffer
Committee Member

_____

Mark A. Bourassa
Committee Member

To Mom and Dad

ACKNOWLEDGEMENTS

TABLE OF CONTENTS

LIST OF FIGURES

ABSTRACT

High-resolution, research-quality surface pressures are objectively calculated over the Southern Ocean from SeaWinds on QuikSCAT winds. The pressure fields are validated in comparison to in situ observations. Overall, the scatterometer-derived surface pressures are a small improvement over the NCEP/NCAR reanalysis, which is used as the objective technique s background field. This improvement is understated primarily because the comparison data undersample storms. Instances are found where the NCEP/NCAR reanalysis misses storms entirely and the scatterometer-derived pressures are a large improvement (as much as 20 mb).

1. INTRODUCTION

The scarcity of observations over the oceans has long frustrated meteorological research in the Southern Hemisphere. Launched in 1999, the SeaWinds scatterometer on the QuikSCAT satellite provides unprecedented coverage of the Southern Ocean (Fig. 1). The SeaWinds scatterometer actively measures radar backscatter at multiple viewing geometries. This information has been used to determine high-quality surface wind speed and direction (Bourassa et al. 1997; Freilich and Dunbar 1999; Bourassa et al. 2001). While these scatterometer winds have been useful to oceanographers in forcing ocean models (e.g., Verschell et al. 1999 or Barnier et al. 1991), surface winds are relatively difficult for meteorologists to interpret and digest. Instead, surface pressures are a more useful product for most meteorologists. This paper examines the calculation of surface pressures from scatterometer winds.

Endlich et al. (1981) were among the first to derive surface pressures from scatterometer wind data. SASS wind measurements were objectively analyzed onto a regular grid. The nonlinear balance equation was then solved to yield surface pressures. They obtained reasonable results, although their method suffered from the deficiency of not accounting for the atmospheric boundary

suffered from the deficiency of not accounting for the atmospheric boundary layer. The boundary layer was accounted for in the work of Brown and Zeng

1

(1994) who inverted a boundary layer model with ERS-1 winds as a lower boundary condition. A pressure field was found with the constraint that it minimized the difference between the geostrophic wind defined by the pressure field and the winds retrieved from inverting the boundary layer model. One weakness of their method was the winds retrieved from the model were closer to gradient winds than to geostrophic winds. This weakness can be removed by applying a gradient wind adjustment (Patoux and Brown 2002).

The method to be used in this paper was originally developed by Harlan and O'Brien (1986), improved by Zierden et al. (2000), and is developed further herewithin. The Harlan and O'Brien method takes a variational approach to smoothly blend vorticity from the scatterometer winds with geostrophic vorticity from an existing pressure analysis. The method accounts for the boundary layer in a simple way that assumes neutral stratification and barotropic conditions. Although these assumptions seem crude, they eliminate the need for upper air or temperature data, which are likely to be seriously inaccurate in the most interesting cases when the scatterometer differs greatly from the existing analysis. Brown and Zeng (1994) found no more than a 2-mb change when baroclinicity and stratification were included than when barotropic and neutral conditions were assumed. The Harlan and O'Brien method also has the strength of not requiring any iteration when applying a gradient wind adjustment as in Patoux and Brown (2002).

(2002).

2

This study has two goals. First is a demonstration that the scatterometer can be effectively used to calculate high-resolution, research-quality surface pressure fields without thousands of buoys. Second is a demonstration that the scatterometer has an impact on existing analysis covering the Southern Ocean. To these ends, the following plan is adopted. The scatterometer data and in situ comparison data is described in section 2. The variational method is developed in section 3. Section 4 compares the calculated scatterometer pressures with in situ comparison data. Small statistical improvements over the existing analysis are found, but it is argued that these improvements are underestimated and this is supported by a brief case study in section 5.
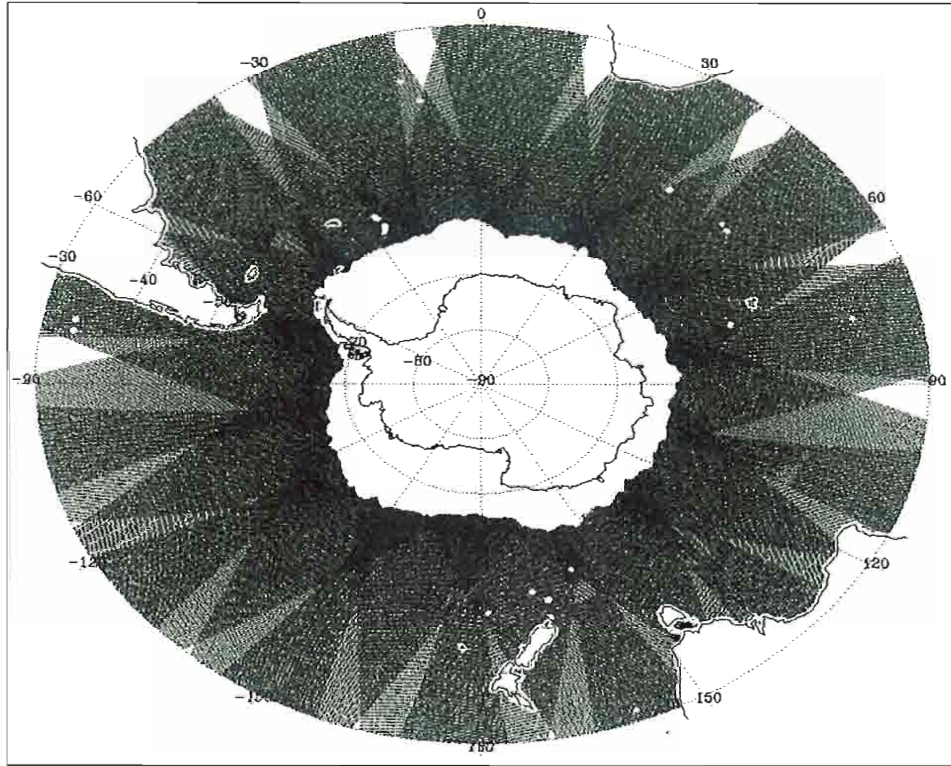
FIG. 1. Illustration of QuikSCAT daily coverage.

2. DATA

QuikSCAT is a sun-synchronous satellite with a period of 101 minutes. The SeaWinds scatterometer uses two conically rotating pencil beams operating in the Ku-band (13.402 GHz). Individual footprints are binned into 25x25 km cells with as many as 76 cells across the satellite swath. A geophysical model function relates the backscatter cross-section to the near surface wind velocity. The data used in this study were processed with the Ku-2001 model function that has been shown to result in 60% of the QSCAT-1 uncertainties (Bourassa et al. 2001). Radiometer data from other satellites were used to flag cells potentially contaminated by precipitation. Radiometer data are considered good where available, but these data are not often available. Flagged cells are not considered in the analysis.

The NCEP/NCAR reanalysis (NCEPR) is used as the background pressure field for the variational method. The reanalysis data are available on a 2.5° global grid at 6-hour intervals. Linear interpolation in time is used to obtain the pressure field corresponding to the time of the QuikSCAT overpass. The NCDC TD1129 marine observations are used as the comparison data in this study. Nearly all of the observations are ship borne. Although these observations may have entered

the NCEPR, they have a small effect on Southern Hemisphere analysis as

5

evidenced by their relatively small correlation (Fig. 2). The fact that some correlation does exist and the comparison data and background field are not completely independent implies that the validation will tend to understate the improvement of the scatterometer-derived pressures over the existing background pressures.
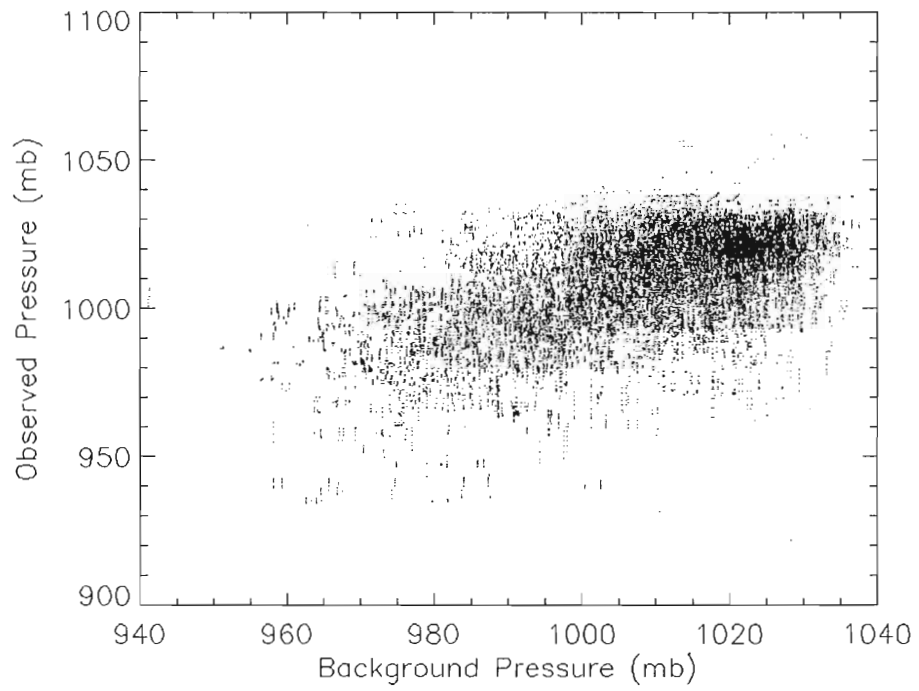
FIG. 2. Plot of the observed pressure against the background pressure ($r^2 = 0.35$, n = 25 721).

3. METHODOLOGY

Surface pressures are calculated from QuikSCAT winds using a variational technique that follows Harlan and O'Brien (1986) and Zierden et al. (2000). The variational method minimizes a cost function

$$F(p_{ij}, \zeta_{ij}, \lambda_{ij}) = \sum_i \sum_j \left[\lambda_{ij} H_{ij} + \frac{K_\zeta}{2} M_{ij}^2 + \frac{K_E}{2} G_{ij} \right]. \tag{1}$$

H_{ij} is the strong constraint or model (Sasaki 1970) and has the form

$$H_{ij} = \frac{1}{\rho f_j} \left(\nabla^2 p_{ij} - \frac{\beta_j}{f_j} \frac{\partial p_{ij}}{\partial y} \right) - \zeta_{ij}, \tag{1}$$

where p_{ij} and ζ_{ij} are the solution pressure and solution geostrophic vorticity fields and f_j and β_j are the Coriolis and beta parameters. λ_{ij} are the Lagrange multipliers. The data misfit term has the form

$$M_{ij} = \zeta_{ij} - \left(\zeta^*_{ij} \right)_g. \tag{2}$$

The geostrophic vorticity from data, $(\zeta^*_{ij})_g$, takes on the satellite value, $(\zeta_{ij}^S)_g$, inside the swath and the background value, $(\zeta_{ij}^B)_g$, outside the swath. The background geostrophic vorticity is easily calculated using the relationship

$$\left(\zeta_{ij}^B \right)_g = \frac{1}{\rho f_j} \left(\nabla^2 p_{ij} - \frac{\beta_j}{f_j} \frac{\partial p_{ij}}{\partial y} \right). \tag{3}$$

$$\left(\zeta_{ij}^B \right)_g = \frac{1}{\rho f_j} \left(\nabla^2 p_{ij} - \frac{\beta_j}{f_j} \frac{\partial p_{ij}}{\partial y} \right). \tag{3}$$

8

Calculation of the geostrophic vorticity from the satellite is more involved and will be described in the next paragraph. Finally, a regularization term is included so that the scatterometer vorticity is blended with the background vorticity. Without such a term, the only solution is $\lambda = 0$ and the satellite vorticity would be inserted directly into the field. There are many choices for regularization, but minimization of the geostrophic kinetic energy has been found to be successful (e.g., Zierden et al. 2000; Harlan and O'Brien 1986):

$$G_{ij} = \frac{1}{2\rho^2 f_j^2} \nabla p_{ij} \bullet \nabla p_{ij} \tag{4}$$

The coefficients K_ζ and K_E are the Gaussian precision modulii, and their ratio controls the relative amounts of smoothing to data misfit. Note that K_ζ and K_E are also required for dimensional homogeneity. All calculations involving the satellite winds are done on the observational grid, which has a regular ~25 km spacing. Delunay triangulation and interpolation (Renka 1982) transfers the background and satellite vorticity onto a regular 0.25° earth-aligned grid just prior to minimizing the cost function.

The satellite winds are adjusted to geostrophic values according to the following procedure. First, a boundary layer adjustment transforms the 10-m equivalent neutral (Verschell et al. 1999) scatterometer winds to gradient winds at the top of the boundary layer. The boundary layer adjustment consists of an anticyclonic rotation of the wind direction by 18° and scaling of the wind speed

9

by 1.5, which were suggested by theoretical considerations for neutral stability and barotropic conditions (Brown and Zeng 1994). Although such a model is simple, it has been found to be very effective (Harlan and O'Brien 1986), and eliminates the reliance on questionable thermal or upper air data that would be required for a more complicated boundary-layer representation. Brown and Zeng (1994) found that inclusion of baroclinicity and stratification never made more than a 2-mb difference in the calculated pressures than when barotropic and neutral conditions were assumed. The gradient winds (V) are then adjusted to geostrophic values (V_g) with a straightforward application of the gradient wind equation

$$V_g = V\left(1 + \frac{V}{fR}\right) = V(1 + Ro)$$

(5)

where Ro is the Rossby number. If the flow is steady, the Appendix shows that

$$Ro = \frac{1}{fV^2}\left[\left(u^2 \frac{\partial v}{\partial x} - v^2 \frac{\partial u}{\partial y}\right) - uv\left(\frac{\partial u}{\partial x} - \frac{\partial v}{\partial y}\right)\right]$$

(6)

More generally, if the flow is not steady, a term involving time derivatives of the wind can be included, but Patoux and Brown (2002) obtained good results without this term. It should be noted that the Rossby number field requires minimal smoothing to make the gradient wind adjustment meaningful. In practice, a 225-km low-pass binomial filter (J hne 1991) is applied to the satellite vorticity and a 325-km low-pass binomial filter is applied to the Rossby number field. Since Ro is calculated from scatterometer winds, no iteration is required as vorticity and a 325-km low-pass binomial filter is applied to the Rossby number field. Since Ro is calculated from scatterometer winds, no iteration is required as in Patoux and Brown (2002).

Minimization of the cost function involves solving

$$\frac{\partial F}{\partial \lambda_{ij}} = H_{ij} = 0,$$
(7)

$$\frac{\partial F}{\partial \zeta_{ij}} = K_\zeta M_{ij} - \lambda_{ij} = 0, \text{ and}$$
(8)

$$\frac{\partial F}{\partial p_{ij}} = \frac{1}{\rho f_j}\left[\nabla^2 \lambda_{ij} + \left(\frac{\beta_j}{f_j}\right)\frac{\partial \lambda_{ij}}{\partial y} + \frac{K_E}{(2pf_j)^2}\nabla^2 p_{ij}\right] = 0.$$
(9)

Eq. (10) has a solution of the form

$$\lambda_{ij} = \left(\frac{K_E}{4\rho f_j}\right)(p_{ij} - p_{0ij}),$$
(10)

Where p_{0ij} is the homogeneous solution. The homogeneous solution satisfies

$$\left(\frac{K_E}{4\rho f_j}\right)\nabla^2 p_{0ij} = 0,$$
(11)

and $\lambda = 0$ on the boundaries implies $p_{0ij} = p_{ij}$. Substituting (11) into (9) gives

$$\zeta_{ij} = \zeta *_{ij} + \left(\frac{K}{2\rho f_j}\right)(p_{ij} - p_{0ij}),$$
(12)

where $K = K_E/2K_\zeta$. Putting (13) into (8) yields

$$\nabla^2 p_{ij} - \left(\frac{\beta_j}{f_j}\right)\frac{\partial p_{ij}}{\partial y} - \left(\frac{K}{2}\right)(p_{ij} - p_{0ij}) = \rho f_j \zeta *_{ij}$$
(13)

Eq. (14) is solved using successive overrelaxation using Neumann boundary conditions. The homogeneous solution is sufficient to determine the additive constant. An optimal relaxation parameter (e.g., Press et al. 1992) of 1.8 is used along with second-order finite difference representations of the derivatives. A constant. An optimal relaxation parameter (e.g., Press et al. 1992) of 1.8 is used along with second-order finite difference representations of the derivatives. A

11

value of K is chosen to produce a sufficiently smooth field while preserving the physical features in the SeaWinds vorticity field. Choosing higher values of K produce smoother isobars and more relaxed gradients. The most appropriate value of K also depends on the grid spacing and on the smoothing and adjustment of the vorticity field prior to solving (14). In practice a value of $K = 5.0 \times 10^{-12}$ m^{-2} is used to produce a smooth pressure field while retaining physical features in the SeaWinds geostrophic vorticity field.

4. VALIDATION

The region used in this study is 30-70°S for the 20-day period 1-20 June 2000. The calculations were performed with individual scatterometer swaths contained within a box extending 5° beyond the maximum and minimum longitude points of the swath. All observations falling within this box and within 3 hours of the satellite overpass are used for validation. The observation locations are given at a resolution of 0.1° and the surface pressures are on 0.25° grids. Bilinear interpolation (e.g., Press et al. 1996) was used to interpolate from the 0.25° grid to the observation location. Thus, the co-location radius was 0.15° latitude ≈ 17 km and 3 hr.

Table 1 shows that, on average, the calculated and background pressures are a few millibars lower than the observed pressures. The statistics in Table 1 are computed at the validation points only. The calculated pressures display a little less variance than the background or observed pressures. The fourth and fifth lines in Table 1 show that the calculated pressures are slightly closer to the observations (in an RMS sense) than the background pressures. This probably understates how much closer the calculated pressures are to the truth. This is observations (in an RMS sense) than the background pressures. This probably understates how much closer the calculated pressures are to the truth. This is because ships tend to avoid storms (Fig. 3), so cases where the scatterometer

identified storms missed in the analysis (e.g., section 5) lack sufficient sampling, furthermore, it is these storms that cause the greatest synoptic scale variability in the surface pressures.

Following Tolman (1998), the model uncertainty (where model means either the calculated or the NCEPR pressures) can be estimated using

$$\langle S'_{mm} \rangle = s_{mm} - [s_{om}^2 / (s_{oo} - \overline{s'}_{oo})] \tag{14}$$

where $\langle S'_{mm} \rangle$ is the expected value of the true model uncertainty, s_{mm} is the estimated model variance, s_{om} is the estimated observation-model covariance, s_{oo} is the estimated observation variance, and $\overline{s'}_{oo}$ is the estimate of the mean observation error. Figure 4 applies eq. (15) for a reasonable range of observational uncertainty. Throughout most of the range, the calculated pressures are about 1.5 mb more accurate than the NCEPR. Note that if the observations were perfect, the calculated pressures would have an uncertainty of about 11.5 mb. One might also ask, if the calculated pressures were perfect, what uncertainty would that imply for the observed pressures? The answer, 13.5 mb, can either be found by deriving an equation similar to (15) for $\langle S'_{mm} \rangle$ or by reading where the calculated curve crosses the abscissa in Fig. 4.

A bin-average analysis (BAA) is used to obtain a more precise idea of the observation and calculated pressure uncertainty, assuming the differences in the mean are relatively small. The BAA examines the functional relationship

mean are relatively small. The BAA examines the functional relationship between the calculated minus observed pressure binned first according to the

calculated pressure and then according to observed pressure. A BAA requires specification of a bin width and minimum number of data per bin. In this study a bin width of 2-mb and minimum number of 60 data per bin are used throughout. If the observation and calculated pressure uncertainties have been accurately deduced, then a BAA using synthetic data should replicate a BAA of the real data (Kent et al. 1998, Kent and Taylor 1999). Reproducibility of the BAA is a necessary, but not sufficient condition for accurate error estimation.

The synthetic data are observed surface pressures for May 2000. The same number of pressures for May 2000 are chosen as validation points in June 2000. The May pressures are then rescaled so that the range and first two moments of the May pressures are more similar to the June pressures. Both the observed and the calculated pressure uncertainties need to be at least 8 mb for the synthetic BAA to have a broad resemblance to real BAA. The synthetic BAA most closely resembles the real BAA for an observed pressure uncertainty of 13.5 mb and calculated pressure uncertainty of 11.5 mb (Fig. 5). Thus, the closest BAA minimizes the calculated pressure uncertainty when considering the observations and minimizes the observation uncertainty when considering the calculated pressures. The closest BAA provides an upper bound for the observed and calculated pressure uncertainties. Thus, one would expect the observed and calculated pressure uncertainties to be no larger than 13.5 and 11.5 mb, respectively. Combining the BAA results with the uncertainty estimate from eq.

respectively. Combining the BAA results with the uncertainty estimate from eq. (15) imply observation and pressure uncertainties somewhere in the upper

15

quadrant of Fig. 4. The calculated pressure uncertainties are smaller than the observation errors for some of this quadrant, but further work would be necessary to determine if this is indeed the case. In any event, it is clear that the SeaWinds calculated pressures are more accurate than the NCEPR.

**TABLE. 1.** Statistics for the calculated, background, and observed pressures and their differences calculated at the validation points (n = 25 731).

Quantity	Mean (mb)	RMS Difference (mb)
Observed	1009.08	16.95
Calculated	1006.09	14.75
Background	1007.62	16.37
Calculated-Observed	-3.00	13.96
Background-Observed	-1.45	15.10
Calculated-Background	-1.55	5.43
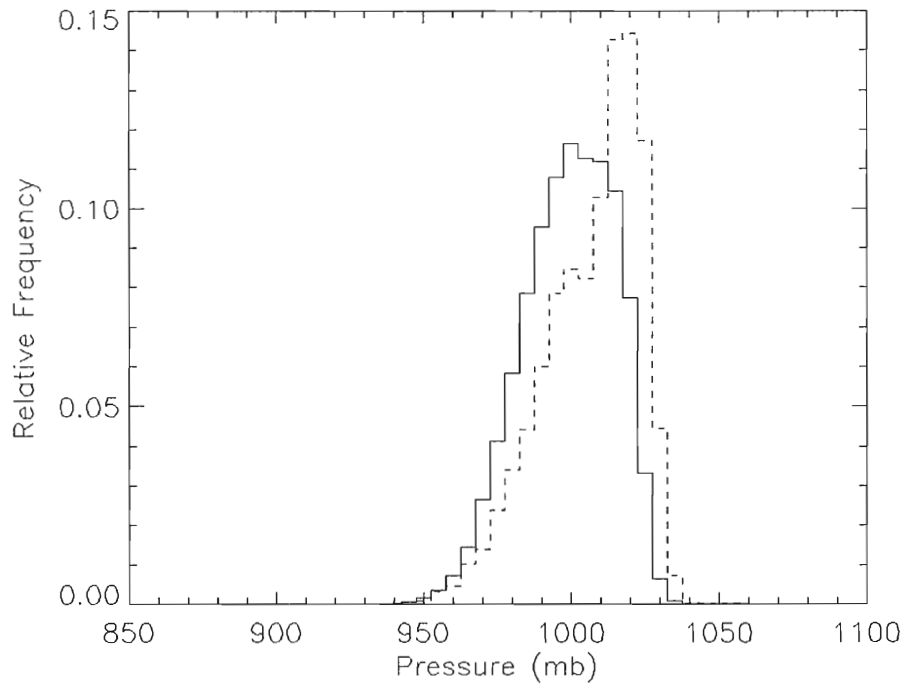
FIG. 3. Histograms for all calculated pressure points (solid) and observation pressure points (dashed). It can be seen that all the calculated pressure points include low pressures not found at the validation (observation) points.
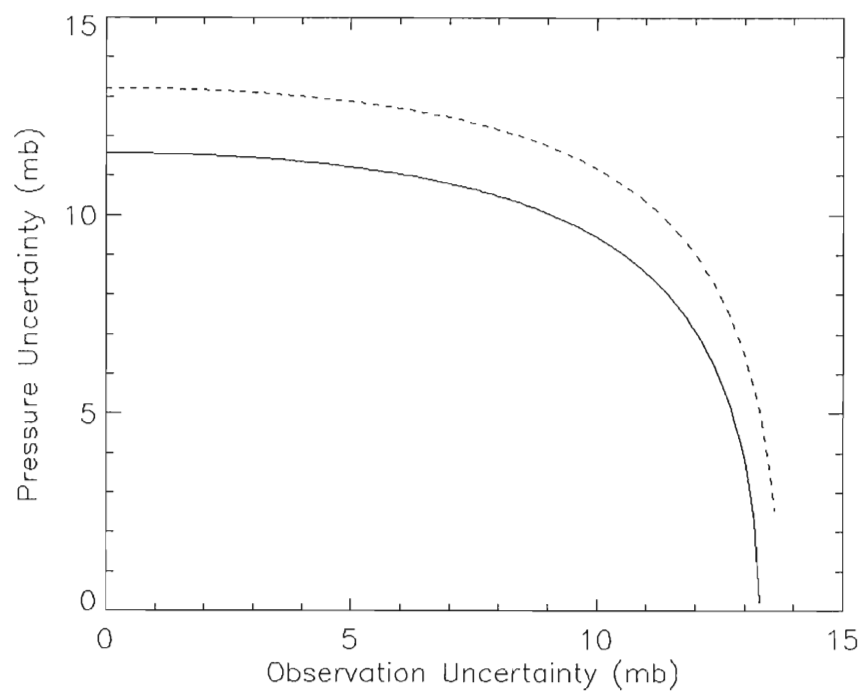
FIG. 4. Estimate of the calculated (solid) and NCEPR (dashed) pressure uncertainty for a range of observational uncertainties.
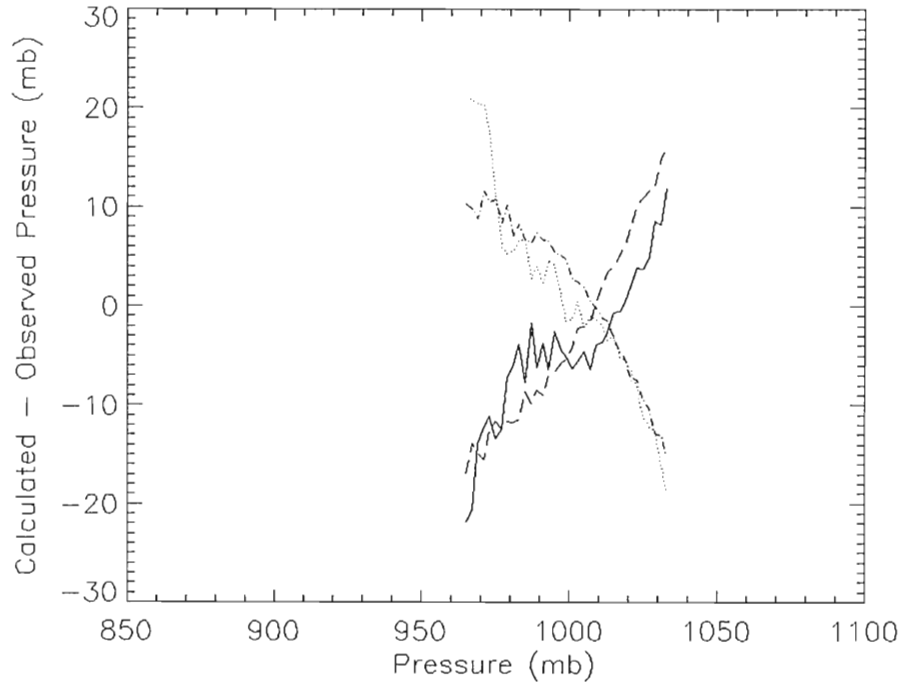
**FIG. 5.** Bin-average analysis using the calculated pressure (solid), observed pressure (dotted), synthetic calculated pressure (long-dash), and synthetic observed pressure (dot-dash). The synthetic data for this figure used a SeaWinds calculated pressure uncertainty of 11.5 mb and an observed pressure uncertainty of 13.5 mb, which are the upper limit on the uncertainties (see text for further explanation).

explanation).

20

5. CASE STUDY

Briefly examining the evolution of one of the storms during the study period is beneficial for understanding NCEPR deficiencies and what SeaWinds on QuikSCAT has to offer. The example also illustrates the good performance of SeaWinds on QuikSCAT in high wind conditions. The example begins on 7 June with a storm that has formed between Australia and Antarctica (Fig. 6). In three days this storm moves eastward by about 30° (Fig. 7). The NCEPR has begun to

recognize this system about to crash into New Zealand, but has a central pressure 16 mb higher than the scatterometer pressure field. Four days later (Fig. 8) after passing New Zealand the NCEPR represents the system much better; however, the NCEPR has missed a system (Fig. 9) that formed just downwind of New Zealand. This cycle begins again with another system forming in the region between Australia and Antarctica (Fig. 10). This system, however, dives southward (Fig. 11) and continues to elude the NCEPR. Other cases similar to this one were also typical between Africa and Antarctica. The relative proximity of these systems to land highlights the importance that they be identified and tracked.
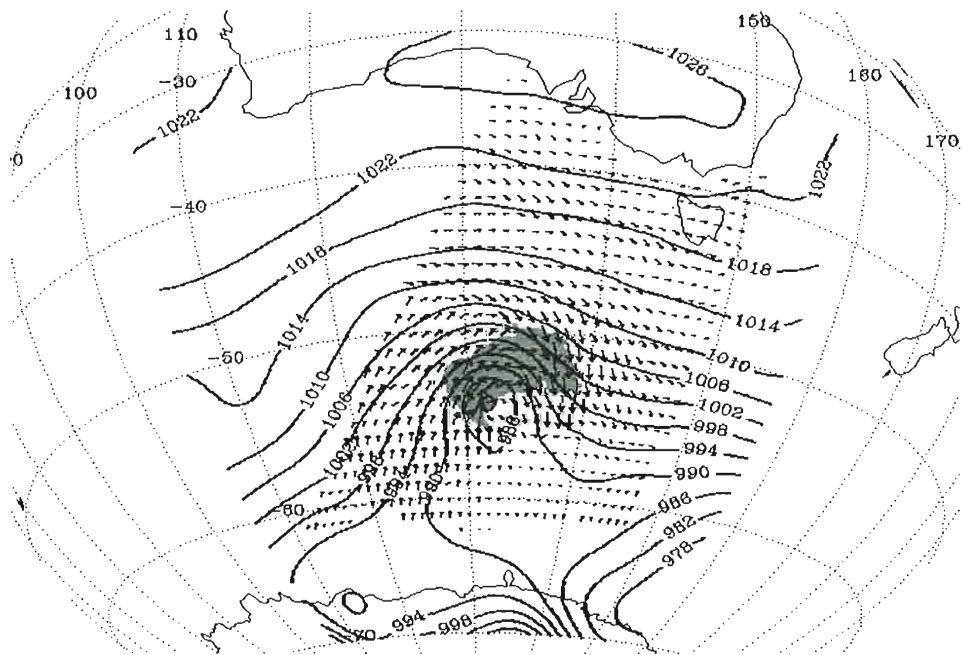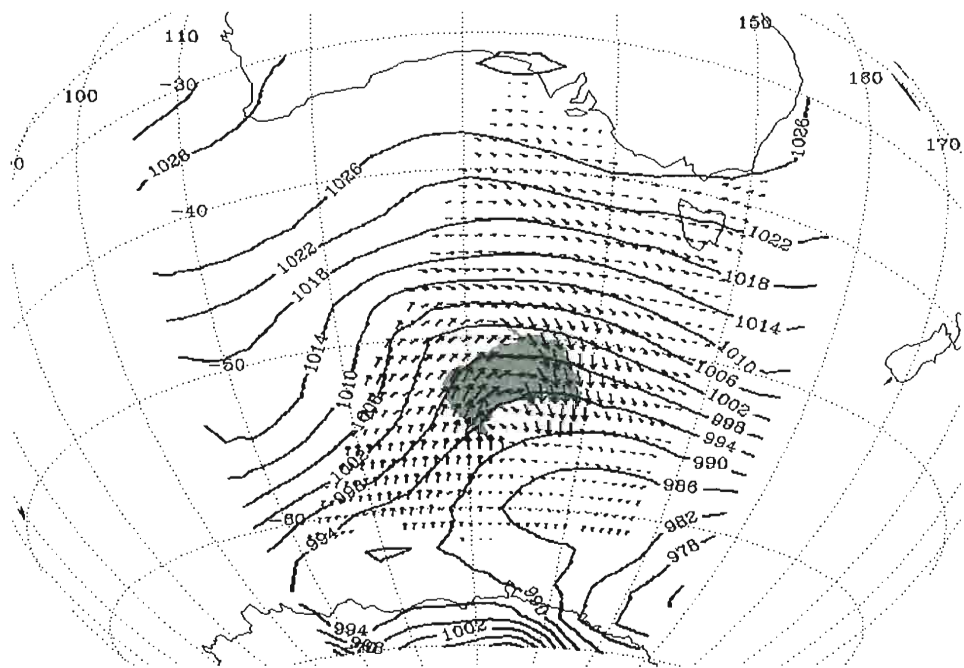
tracked.

FIG. 6. SeaWinds winds (greater than 35 kts shaded) with NCEPR pressures
(top) and calculated pressures (bottom) for 7 June 2000. The southern limit of the

FIG. 6. SeaWinds winds (greater than 35 kts shaded) with NCEPR pressures
(top) and calculated pressures (bottom) for 7 June 2000. The southern limit of the
swath indicates the location of the ice edge.

22

FIG. 7. SeaWinds winds (greater than 35 kts shaded) with NCEPR pressures (top) and calculated pressures (bottom) for 10 June 2000.
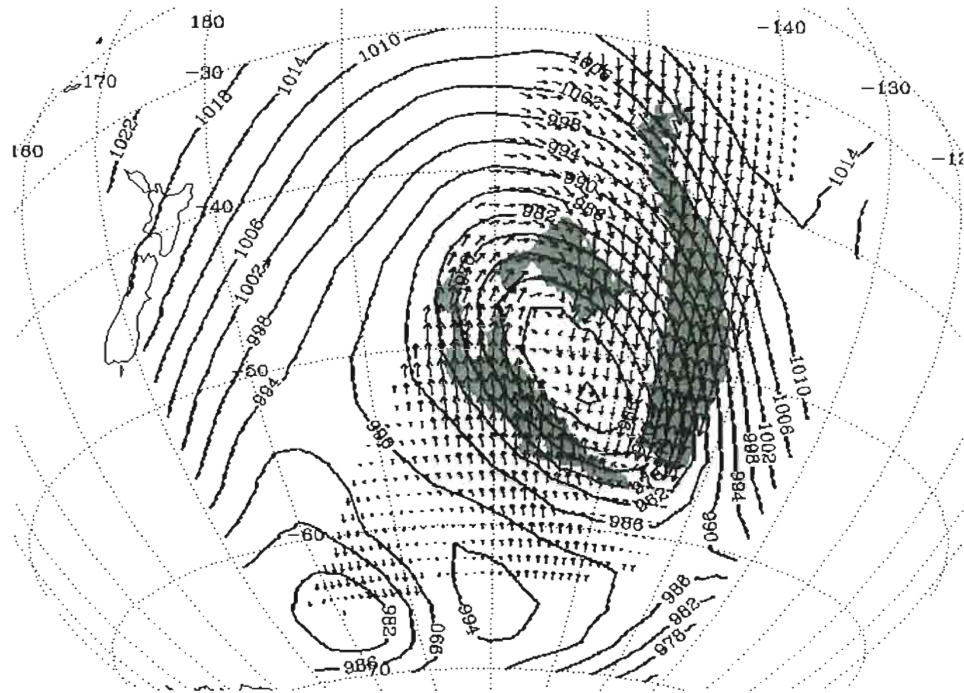
FIG. 8. SeaWinds winds (greater than 35 kts shaded) with NCEPR pressures (top) and calculated pressures (bottom) for 14 June 2000.

24

FIG. 9. SeaWinds winds (greater than 35 kts shaded) with NCEPR pressures (top) and calculated pressures (bottom) for 14 June 2000.

25

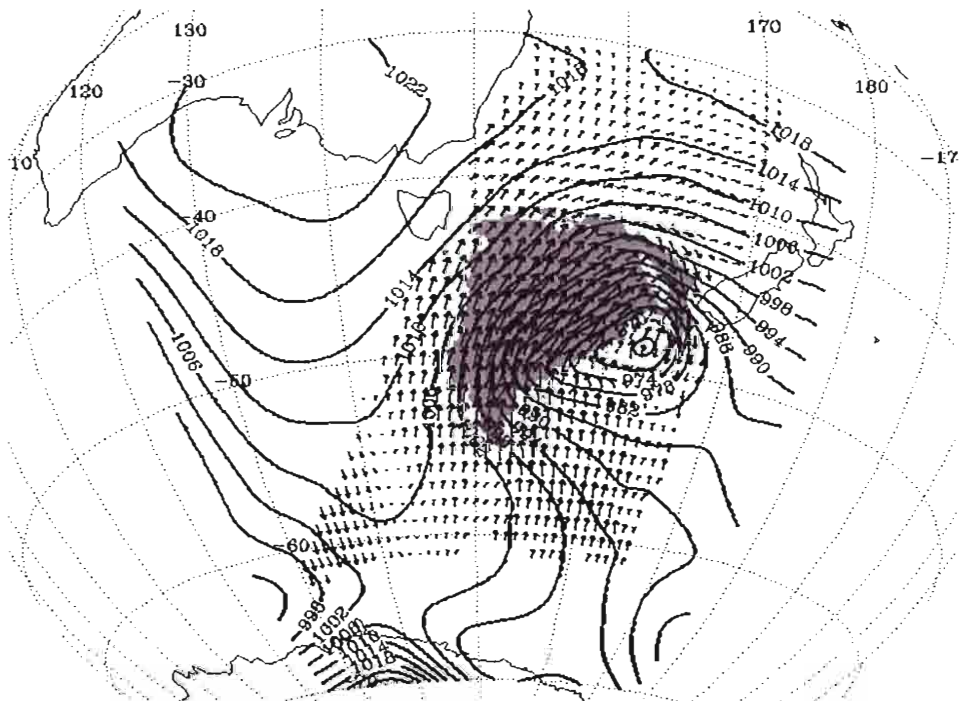**FIG. 10.** SeaWinds winds (greater than 35 kts shaded) with NCEPR pressures (top) and calculated pressures (bottom) for 17 June 2000.
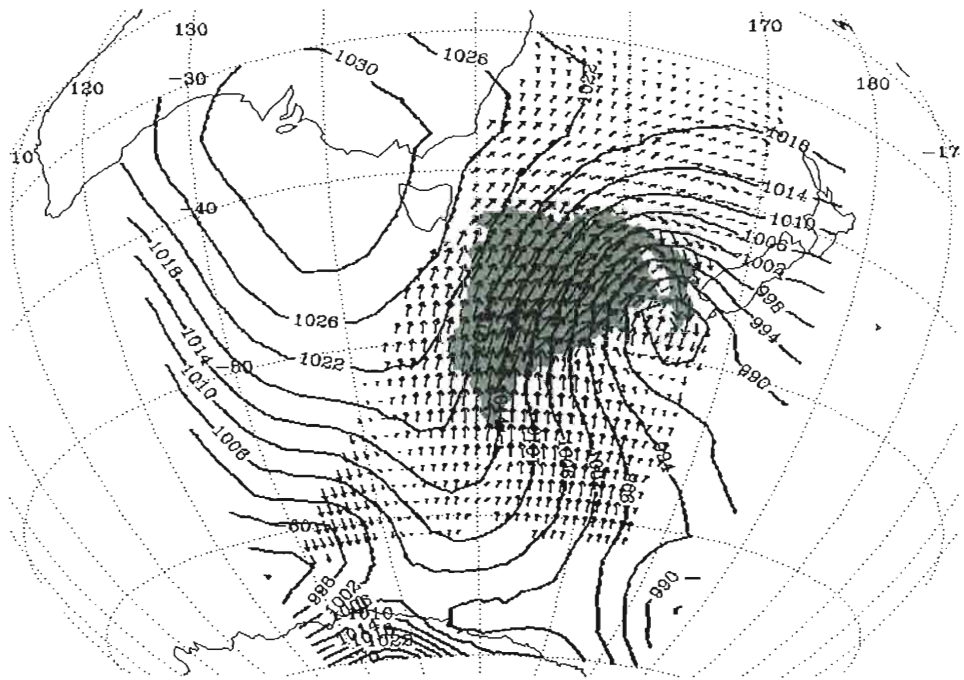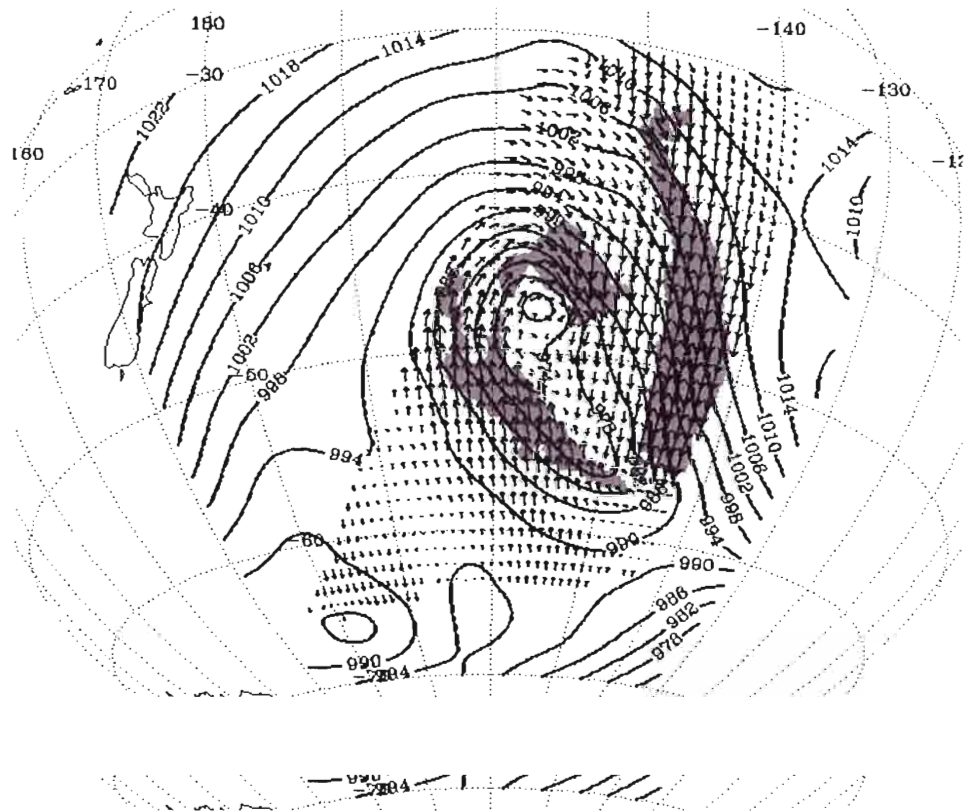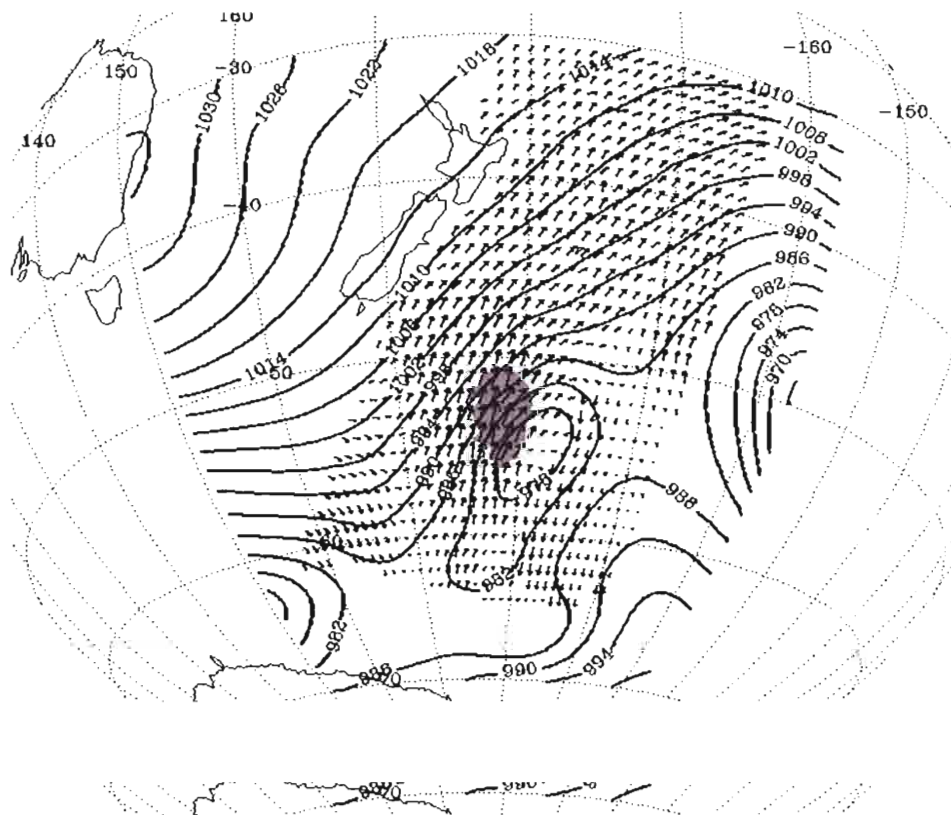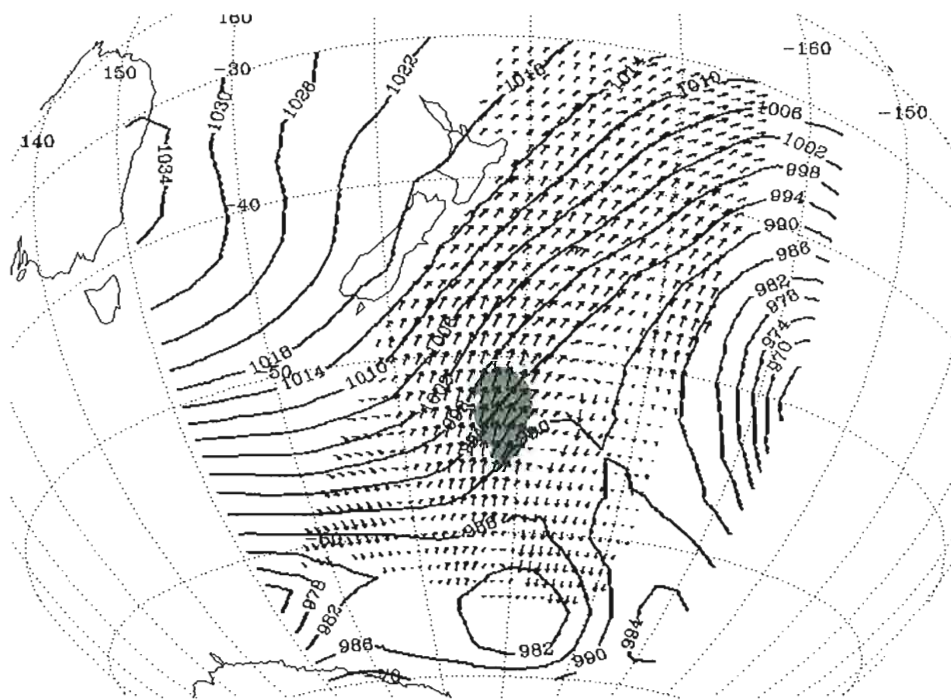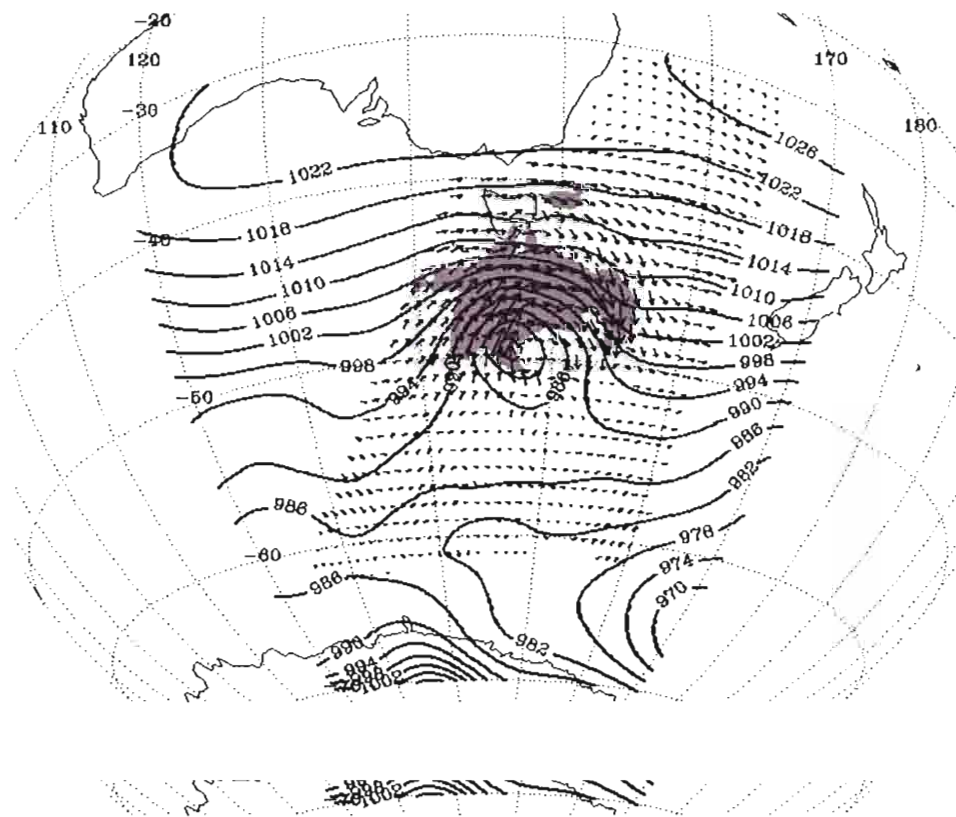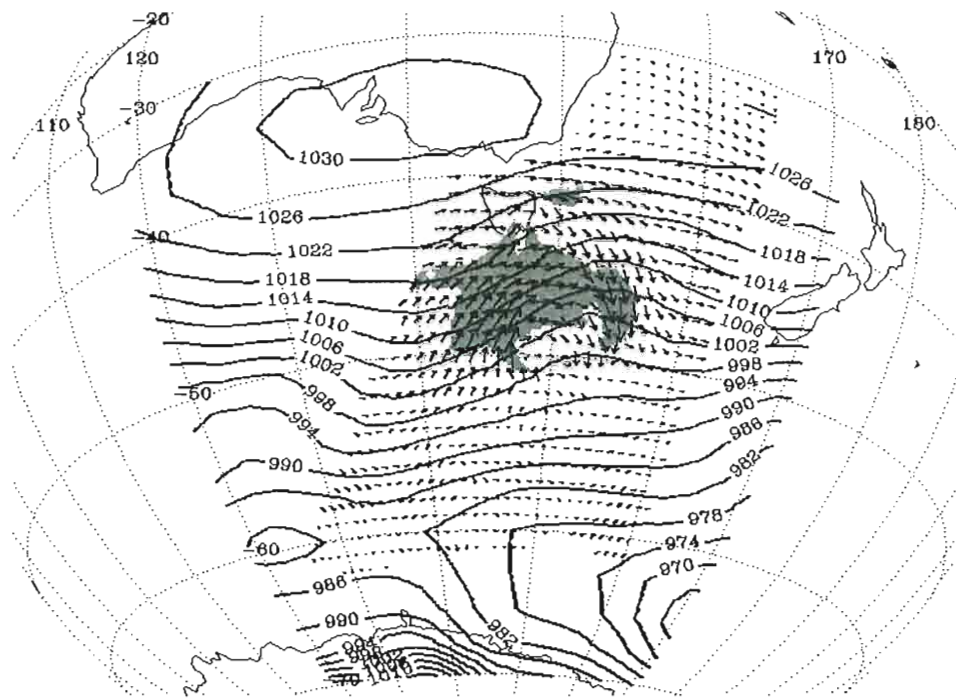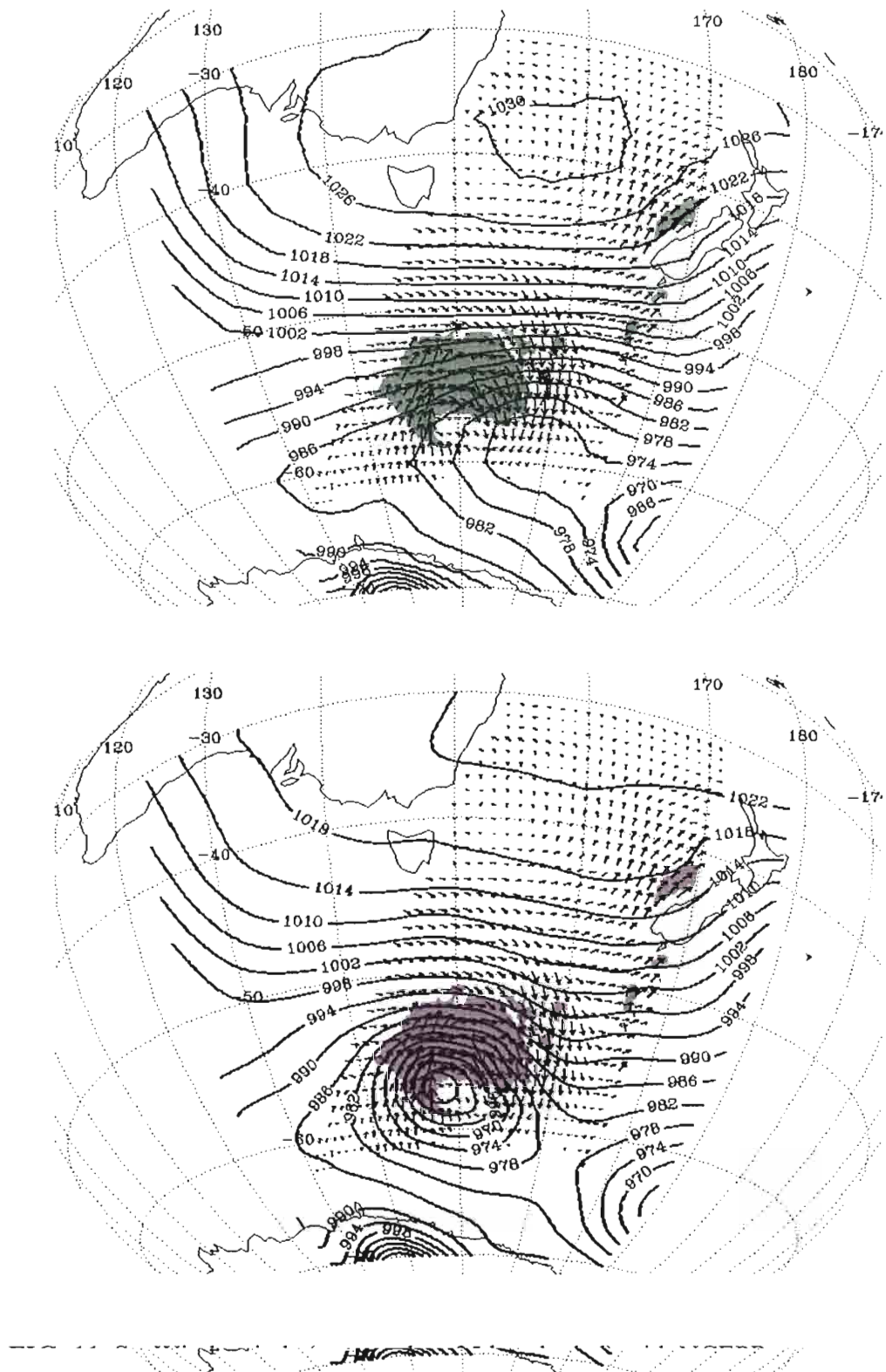
26

FIG. 11. SeaWinds winds (greater than 35 kts shaded) with NCEPR pressures (top) and calculated pressures (bottom) for 18 June 2000.

27

6. CONCLUSIONS

This study has shown that the scatterometer can be effectively used to calculate high-resolution, research-quality surface pressures. This study has also shown that the scatterometer can improve upon the existing (NCEPR) analysis covering the Southern Ocean. Quantitatively, it was found that surface pressures calculated from SeaWinds on QuikSCAT winds provide a small improvement over the NCEPR. The tendency for ships to avoid storms, however, makes it likely that the true improvement is much greater, and this study presents an example showing that the SeaWinds pressures appear to be a large improvement over the NCEPR. It should be noted that the example of NCEPR missing entire storms is typical for the Southern Ocean, and a case of potential importance to the people of Australia and New Zealand. Beyond forecasting, the SeaWinds pressures can be used to examine many different questions. The SeaWinds pressures can be used to estimate how much the NCEPR underestimates the eddy flux statistics over the Southern Hemisphere. The SeaWinds pressures would make an interesting comparison dataset for examining the differences between the Australian Bureau of Meteorology's analysis and the NCEPR. This study might also be repeated with the background from the ECMWF analyses, which are used

also be repeated with the background from the ECMWF analyses, which are used by the altimetry community. It would be interesting to assess the magnitude of

28

the impact that SeaWinds pressures have on the inverse barometer correction for altimetry work. Finally, the SeaWinds pressures can also be used to study the occluding stage lows over the Southern Ocean.

APPENDIX

THE GRADIENT WIND ADJUSTMENT

Begin by defining $s(t)$, the position along a curve traced by a parcel, i.e.,

$$s(t) = \| \mathbf{X}(t) - \mathbf{X}(t_0) \|.$$

Also define $V(x, y, t)$ to be the speed of the parcel at every point along s. Thus,

$$Ds/Dt = V(x, y, t).$$

Defining $\theta(x, y, t)$ to be the angular direction of the wind in the mathematical

convention (θ is measured counter-clockwise from the x-axis), implies that

$$\partial\theta/\partial s = R_S^{-1} \quad \text{and} \quad D\theta/Ds = R_T^{-1}$$

where R_S is the radius of curvature of the streamlines and R_T is the radius of

curvature of the trajectories. Therefore,

$$D\theta/Dt = (D\theta/Ds)(Ds/Dt) = V/R_T.$$

Also,

$$D\theta/Dt = (\partial/\partial t + V \partial/\partial s + w \partial/\partial z)\theta \approx \partial\theta/\partial t + V/R_S.$$

For practical use, the vertical advection of curvature must be neglected. If

vertical motion is present, the actual 3-dimensional trajectories tend to by less

cyclonic than the trajectories estimated on isobaric charts (Endlich 1961). Hence,
vertical motion is present, the actual 3-dimensional trajectories tend to by less

cyclonic than the trajectories estimated on isobaric charts (Endlich 1961). Hence,

$$\partial\theta/\partial t = V(R_T^{-1} - R_S^{-1})$$

or

$$R_T^{-1} = V^{-1}\partial\theta/\partial t + \partial\theta/\partial s$$

which are both forms of Blaton's Equation. If the local turning of the wind is zero (for example, a disturbance is not translating), then the radius of curvature of the trajectories is the same as the radius of curvature of the streamlines and $Ro = V/(f\,\partial\theta/\partial s)$.

The chain rule implies

$$\partial\theta/\partial s = (\partial x/\partial s)(\partial\theta/\partial x) + (\partial y/\partial x)(\partial\theta/\partial y)$$

and noting that

$$\partial x/\partial s = \cos\theta \quad \text{and} \quad \partial y/\partial x = \sin\theta$$

gives

$$\partial\theta/\partial s = \cos\theta\,(\partial\theta/\partial x) + \sin\theta\,(\partial\theta/\partial y)$$

Trigonometry gives

$$\tan\theta = v/u, \quad \sin\theta = v/V, \quad \text{and} \quad \cos\theta = u/V$$

whose signs are correct in all four quadrants. Thus

$$Ro = V/f[\,(u/V)\,\partial(\arctan(v/u))/\partial x + (v/V)\,\partial(\arctan(v/u))/\partial y]$$

Therefore

$$Ro = 1/fV^2[(u^2\,\partial v/\partial x - v^2\,\partial u/\partial y) - uv\,(\partial u/\partial x - \partial v/\partial y)]$$

Therefore

$$Ro = 1/fV^2[(u^2\,\partial v/\partial x - v^2\,\partial u/\partial y) - uv\,(\partial u/\partial x - \partial v/\partial y)]$$

31

Note that this equation is equivalent to the equations in Patoux and Brown (2002) and Endlich (1961) through constant-f geostrophy.

In performing the gradient wind adjustment, the geostrophic wind takes the form

$$\mathbf{V_g} = (u(1+Ro),\ v(1+Ro))$$

And the geostrophic vorticity takes the form

$$\zeta_g = \zeta\,(1+Ro) + v\,\partial(Ro)/\partial x - u\,\partial(Ro)/\partial y$$

Cyclonic curvature has $Ro > 0$ so that $V_g > V$, while anticyclonic curvature has $Ro < 0$ giving $V_g < V$ (these are true in both hemispheres). Note that vorticity will undergo a large adjustment both where the curvature (R^{-1}) is large (e.g., a tight low) and where the curvature changes rapidly ($\partial R^{-1}/\partial x, y$ is large) even when the curvature (R^{-1}) is not necessarily large (e.g., along the axis of a jet).

REFERENCES

Barnier, B., M. Boukthir, and J. Verron, 1991: Use of satellite scatterometer winds to force and ocean general-circulation model. *J. Geophys. Res. Oceans*, **96**, 22025-22042.

Bourassa, M. A., M. H., Freilich, D. M. Legler, W. T. Liu, and J. J. O'Brien, 1997: Wind observations from new satellite and research vessels agree. *EOS Trans. Amer. Geophys. Union*, 587&602.

Bourassa, M. A., D. M. Legler, J. J. O'Brien, and S. R. Smith, 2002: SeaWinds validation with research vessels. *J. Geophys. Res.*, in press.

Brown, R. A., and L. Zeng, 1994: Estimating central pressures of oceanic midlatitude cyclones. *J. Appl. Meteor.*, **33**, 1088-1095.

Endlich, R. M., D. E. Wolf, C. T. Carlson, J. W. Maresca, Jr, 1981: Oceanic wind and balanced pressure-height fields derived from satellite measurements. *Mon. Wea. Rev.*, **109**, 2009-2016.

Endlich, R. M., 1961: Computation and uses of gradient winds. *Mon. Wea. Rev.*, **89**, 187-191.

Harlan, J, Jr., and J. J. O'Brien, 1986: Assimilation of scatterometer winds into surface pressure fields using a variational method. *J. Geophys. Res.*, **91**, 7816-7836.

J hne, B., 1991: *Digital image processing: concepts, algorithms, and scientific applications*. Springer-Verlag. 383 pp.

Freilich, M. H., and R. S. Dunbar, 1999: The accuracy of the NSCAT1 vector winds: comparisons with National Data Center buoys. *J. Geophys. Res.*, **104,** 11231-11246.

Kent, E. C., and P .K. Taylor, 1999: Accounting for random errors in linear regression: A practical guide. *Q. J. R. Meteorol. Soc.*, **125**, 2789-2790.

Kent, E. C., and P .K. Taylor, 1999: Accounting for random errors in linear regression: A practical guide. *Q. J. R. Meteorol. Soc.*, **125**, 2789-2790.

Kent, E. C., P. K. Taylor, and P. G. Challenor, 1998: A comparison of ship- and scatterometer-derived wind speed data in open ocean and coastal area. *Int. J. Remote Sensing*, **19**, 3361-3381.

Patoux, J. and R. A. Brown, 2002: A gradient wind correction for surface pressure fields retrieved from scatterometer winds. *J. Appl. Meteor.*, **42**, 133-143.

Press, W. H., S. A. Teukolsky, W. T. Vetterling, B. P. Flannery, 1992: *Numerical Recipes in FORTRAN: The Art of Scientific Computing.* 2nd Ed. Cambridge University Press. 963 pp.

Renka, R., 1982: Interpolation of data on the surface of a sphere, Oak Ridge Nat. Lab. Rep. OLNR/CSD-108.

Sasaki, Y., 1970: Some basic formalisms in numerical variational analysis. *Mon. Wea. Rev.*, **108**, 875-883.

Tolman, H. L., 1998: Effects of observation errors in linear regression and bin-average analysis. *Q. J. R. Meteorol. Soc.*, **124**, 897-917.

Verschell, M. A., M. A. Bourassa, D. E. Weissman, and J. J. O'Brien, 1999: Ocean model validation of the NASA scatterometer winds. *J. Geophys. Res. Oceans*, **104**, 11359-11373.

Zierden. D. F., M. A. Bourassa, and J. J. O'Brien, 2000: Cyclone surface pressure fields and frontogenesis from NASA scatterometer (NSCAT) winds. *J. Geophys. Res.*, **105**, 23967-23981.

BIOGRAPHICAL SKETCH

Personal Information

Born 17 December 1977 in Fairmont, Minnesota

Education

2000 B. S. Atmospheric Sciences (summa cum laude),
University of North Dakota

Fellowships/Scholarships

2001-2002 NASA/Earth Science Enterprise Graduate Fellowship

2000-2001 American Meteorological Society Graduate Fellowship

1998-2000 American Meteorological Society Undergraduate
Fellowship (with Kavouras)

1996-2000 University of North Dakota Presidential Academic
Scholarship

Honors

2001 AGU Outstanding Student Paper Award (Ocean Sciences Section)

2000 University of North Dakota Department of Atmospheric Sciences
Outstanding Student Overall

2000 University of North Dakota Department of Atmospheric Sciences
Outstanding Student Researcher

1999 University of North Dakota Department of Atmospheric Sciences
Outstanding Student Researcher

1999 University of North Dakota Department of Atmospheric Sciences
Outstanding Student Researcher

1998   University of North Dakota Department of Atmospheric Sciences
Outstanding Sophomore

1998   Studio One Exceptional Performance Award

Publications

Hilburn, K. A., M. A. Bourassa, and J. J. O'Brien, 2002: Development of
scatterometer derived research-quality surface pressure fields for
the Southern Ocean. Paper 2.14 at 18th Conference on IIPS at 82nd
Annual AMS Meeting, page 30.

Hilburn, K. A., M. A. Bourassa, and J. J. O'Brien, 2001: Development of
scatterometer-derived research-quality surface pressures. *Eos.
Trans. AGU*, 82(47), Fall. Meet. Suppl. Abstract OS31A-0390,
page F625.

Hilburn, K. A., M. R. Poellot, and W. P. Arnott, 2000: The microphysical
structure of aged, mid-latitude, continental anvil cirrus: Three
cases from ARM 1994. *J. Appl. Meteor.*, submitted.

Hilburn, K. A., M. R. Poellot, and W. P. Arnott, 2000: The microphysical
structure of anvil cirrus: Three cases from ARM 1994.
Proceedings of the Tenth Annual ARM Science Team Meeting.

Poellot, M. R., K. A. Hilburn, W. P. Arnott, and K. Sassen, 1999: In situ
observations of cirrus clouds from the 1994 ARM RCS IOP.
Proceedings of the Ninth Annual ARM Science Team Meeting.

Professional Experience

1999-2000   Data Technician for the University of North Dakota
Department of Atmospheric Sciences

1998   Studio One On-Air Weather Anchor

1998   National Weather Service Student Volunteer

1997   Studio One Weather Team

1997   Studio One Weather Team

1997   Regional Weather Information Center Volunteer Broadcast
Assistant

Memberships

American Geophysical Union

American Meteorological Society

Golden Key

Phi Eta Sigma